Multi-Star Wavefront Control for the Wide-Field Infrared Survey Telescope

Dan Sirbu[1,2], Ruslan Belikov[1], Eduardo Bendek[1,2], Chris Henze, AJ Riggs[3], Stuart Shaklan[3]

[1] NASA Ames Research Center, Moffett Field, Mountain View, CA

[2] Bay Area Environmental Research Institute, Moffett Field, Mountain View, CA

[3] Jet Propulsion Laboratory, California Institute of Technology, Pasadena, CA

ABSTRACT

The Wide-Field Infrared Survey Telescope (WFIRST) is planned to have a coronagraphic instrument (CGI) to enable high-contrast direct imaging of exoplanets around nearby stars. The majority of nearby FGK stars are located in multi-star systems, including the Alpha Centauri stars which may represent the best quality targets for the CGI on account of their proximity and brightness potentially allowing the direct imaging of rocky planets. However, a binary system exhibits additional leakage from the off-axis companion star that may be brighter than the target exoplanet. Multi-Star Wavefront Control (MSWC) is a wavefront-control technique that allows suppression of starlight of both stars in a binary system thus enabling direct imaging of circumstellar planets in binary star systems such as Alpha Centauri.

We explore the capabilities of the WFIRST CGI instrument to directly image multi-star systems using MSWC. We consider several simulated scenarios using the WFIRST CGI's Shaped Pupil Coronagraph Disk Mask. First, we consider close binaries such as Mu Cassiopeia that require no modifications to the WFIRST CGI instrument and can be implemented as a purely algorithmic solution. Second, we consider wide binaries such as Alpha Centauri that require a diffraction grating to enable suppression of the off-axis starlight leakage at Super-Nyquist separations. We demonstrate via simulation dark holes in 10% broadband compatible with the WFIRST CGI.

Keywords: High-Contrast Imaging, Binary Stars, Wavefront Control, WFIRST, Multi-Star Wavefront Control, Super-Nyquist Wavefront Control

1. INTRODUCTION

The main challenge associated with the direct imaging of exoplanets is the suppression of both diffracted and scattered light from the host star so that the dim planetary companion can be imaged at sufficiently small angular separations and contrast ratios.[1] A number of planned space missions including the Wide Field Infrared Survey Telescope (WFIRST), the Habitable Exoplanet Imaging Mission (HabEx), and the Large UV/Optical/Infrared Surveyor (LUVOIR) are planning internal coronagraph instrument to enable direct imaging of nearby star systems to detect and characterize their planetary systems. In particular the WFIRST mission has a planned technology-demonstrator coronagraph instrument (CGI) with an Integral Field Spectrometer (IFS)[?] which has undergone several rounds of testing to demonstration high-contrast in space-relevant conditions.

A coronagraph consists of a set of internal optics that apply phase and amplitude changes at the image and pupil planes of the telescope to enable high-contrast imaging. Coronagraphs are designed to suppress diffraction due to the telescope aperture (including secondary and obscurations) but additional wavefont errors introduced by surface aberrations of can limit performance several orders of magnitude above the theoretical coronagrah design. To recover a region of high-contrast (called the *dark hole*) among a limited-contrast speckle-field created by the presence of optical aberrations, techniques from adaptive optics have been used in conjunction with deformable mirrors (DM).[2] Thus, currently baselined coronagraph designs include a wavefront control (WFC) loop using DMs to enable the creation of high-contrast dark holes.

Multi-star systems, however, pose additional challenges for a coronagraphic starlight suppression system due to the combined off-axis star's diffraction and aberration leakage into the dark hole. As a result, many multi-star

systems are considered unsuitable for direct imaging and not included in direct imaging survey target lists, even though the majority of Sun-like (FGK) stars belong to multistar systems. Alpha Centauri, the nearest star system to the Sun, is an example of a star system excluded from high-contrast imaging surveys since it is a binary system.

Multi-star wavefront control (MSWC) is a wavefront control technique that deals with the additional leakage from the off-axis star to enable direct imaging of exoplanets around binary star systems. This technique was introduced and then detailed elsewhere.[3,4] This study builds on our previous investigation of SNWC with WFIRST for stashades[5] and outlines the compatibility and applicability of MSWC to the WFIRST coronagraph instrument only (without a starshade). We review nearby binary targets (including Alpha Centauri) that would benefit from this technique in Section 2. Section 3 reviews the basic principles of MSWC, identifies the Shaped Pupil Coronagraph's Disk-Science mode as most favourable for imaging Alpha Centauri, and briefly outlines hardware requirements. Finally, we present simulated scenarios of imaging both the Alpha Centauri as system an example of operation of MSWC in the Super-Nyquist mode (MSWC-s) and Mu-Cassiopeia in the Sub-Nyquist mode (MSWC-0). These simulated scenarios study shows that in principle, MSWC is compatible with the WFIRST CGI instrument.

2. MULTI-STAR IMAGING SCIENCE WITH WFIRST

Nearly one half of FGK stars are located in multi-star systems as has been shown by surveys of nearby star systems. Of the nearest 20 FGK stars, 13 are located within multi-star systems as shown in Table 1. These nearby systems are particularly interesting targets for the WFIRST CGI on account of their proximity as their increased photon flux can result in better signal-to-noise ratios for imaging and characterization for finite observation times. Additionally, based on follow-up surveys of host stars of Kepler candidates it has been established that planets around binary stars are relatively common and may be as common as around single-stars. Within 10 pc, 42 out of 67 FGK stars are located in dynamical multi-star systems.

The off-axis companion introduces additional leakage in the dark-hole being surveyed around the on-axis (target) star. The amount of leakage is likely dominated by aberrations at optical surface on the primary and secondary mirrors as well as any additional imaging optics inside the coronagraph instrument. These off-axis speckles are caused by the high-frequency components of the optical aberrations corresponding to the separation to the binary companion. Thus, the intensity of the off-axis speckles is determined by (1) the brightness ratio between the target star and its off-axis companion, (2) the angular separation to the binary companion, and (3) the particular power spectral density (PSD) distribution corresponding to the spatial frequencies across the region of interest. The off-axis leakage for all binary stars within 10 pc is computed taking into account the binary star properties and based on a nominal PSD featuring $\lambda/20$ RMS errors following a f^{-3} power law in Figure 2. Also shown is the 48 x 48 DM's Nyquist limit at 24 λ/D.

The expected leakage is also listed for the nearest binaries for this nominal PSD in Table 1. Thus, 9 out of 13 nearby binary stars are expected to be limited by their off-axis companion's leakage at a contrast of 1e-9 at least for this nominal level of optical aberrations. A few binary stars that are of particular interest are Alf Cen A and B, 61 Cyg A and B, 70 Oph A and B, 36 Oph A and B, and Eta Cas A and B. Alf Cen A and B, Eta Cas A, Alf Cmi A, and 70 Oph A are binaries which are either sufficiently close or sufficiently hot stars such that their habitable zones fall within the WFIRST CGI instrument's field of view.

The Alpha Centauri system is particularly interesting as it is the nearest star system and both binary stars are targets of interest. This means that the habitable zone can be resolved at high spatial resolution. If allocated sufficient observation time, the WFIRST CGI instrument may be able to image rocky planets around these stars if the companion's off-axis leakage can be suppressed to the WFIRST CGI's expected raw contrast level. The Alpha Centauri stars feature an eccentric orbit with an 80 year period leading to stellar separations varying between 11-36 AU. Dynamical studies of the stability regions around the Alpha Centauri stars have shown placed outer stability limits for the semi-major axes for a circumstellar exoplanet's orbit about Alpha Centauri A or B if 2.78 ± 0.65 AU and 2.49 ± 0.71 AU respectively. Thus the entire habitable zone is stable. Additionally, only maximum inclinations of 60° in the plane on the binary are likely which puts constraints on the maximum and location of the dark hole necessary to survey the star system.

#	name	sptype	Vmag	dist (pc)	IHZ (AU)	IHZ (ld)	OHZ (AU)	OHZ (ld)	Mag Pri	Mag Sec	Sep (as)	Sep (L/D)	Comp. Leak.
1	**alf Cen A**	**G2V**	**0.01**	**1.32**	**1.13**	**15.31**	**2.08**	**28.13**	**0.01**	**1.33**	**4.00**	**71.60**	**6.73E-08**
2	**alf Cen B**	**K1V**	**1.33**	**1.25**	**0.60**	**8.58**	**1.12**	**16.04**	**1.33**	**0.01**	**4.00**	**71.60**	**7.64E-07**
3	eps Eri	K2V	3.73	3.22	0.51	2.84	0.95	5.31	**3.73**	17.30	17.10	306.10	2.48E-14
4	**61 Cyg A**	**K5Ve**	**5.21**	**3.49**	**0.29**	**1.48**	**0.56**	**2.85**	**5.21**	**6.05**	**31.40**	**562.09**	**1.73E-10**
5	**61 Cyg B**	**K7Ve**	**6.05**	**3.49**	**0.29**	**1.48**	**0.56**	**2.85**	**6.05**	**5.32**	**31.40**	**562.09**	**7.36E-10**
6	**alf Cmi A**	**F5IV**	**0.37**	**3.51**	**2.37**	**12.06**	**4.25**	**21.64**	**0.37**	**10.80**	**3.80**	**68.02**	**2.09E-11**
7	eps Ind	K5V	4.69	3.62	0.38	1.86	0.72	3.55					
8	tau Cet	G8.5V	3.50	3.65	0.63	3.08	1.15	5.66					
9	HD 88230	K8V	6.61	4.87	0.21	0.78	0.42	1.53					
10	**omi02 Eri**	**K0.5V**	**4.43**	**4.98**	**0.57**	**2.04**	**1.06**	**3.79**	**4.43**	**11.47**	**8.30**	**148.58**	**1.18E-10**
11	**70 Oph A**	**K0-V**	**4.12**	**5.09**	**0.67**	**2.36**	**1.25**	**4.40**	**4.12**	**6.17**	**6.50**	**116.36**	**1.81E-08**
12	**70 Oph B**	**K4V**	**6.17**	**5.09**	**0.23**	**0.82**	**0.44**	**1.55**	**6.17**	**4.12**	**6.50**	**116.36**	**7.86E-07**
13	**36 Oph A**	**K2V**	**5.12**	**5.46**	**0.46**	**1.52**	**0.86**	**2.83**	**5.12**	**5.08**	**5.10**	**91.29**	**1.88E-07**
14	**36 Oph B**	**K1V**	**5.08**	**5.98**	**0.51**	**1.52**	**0.95**	**2.83**	**5.08**	**5.12**	**5.10**	**91.29**	**1.75E-07**
15	sig Dra	G9V	4.68	5.75	0.58	1.81	1.07	3.34	4.68	21.70	11.00	196.91	4.32E-15
16	**HD 131977**	**K4V**	**5.72**	**5.84**	**0.38**	**1.16**	**0.73**	**2.23**	**5.72**	**9.80**	**0.20**	**3.58**	**2.63E-03**
17	**eta Cas A**	**G0V**	**3.52**	**5.95**	**0.98**	**5.03**	**1.78**	**9.12**	**3.52**	**7.51**	**12.90**	**230.92**	**7.95E-10**
18	**eta Cas B**	**K7Ve**	**7.51**	**5.95**	**0.17**	**0.52**	**0.34**	**1.02**	**7.51**	**3.51**	**12.90**	**230.92**	**1.24E-06**
19	V2215 Oph	K5V	6.34	5.97	0.29	0.88	0.56	1.69					
20	**HD 191408 A**	**K2.5V**	**5.32**	**6.02**	**0.41**	**1.23**	**0.74**	**2.20**	**5.32**	**11.50**	**4.30**	**76.97**	**1.16E-09**

Figure 1: Summary of the nearest 20 FGK stars listed by distance (dist) and showing spectral type (sptype), visual magnitude (vmag) and indicating binary properties including magnitude of the primary and secondary components, their last measured separation, and nominal expected leakage (from their binary companion). 13 out of these 20 stars are located in binary star systems and denoted in bold type. Also computed are the expected inner (IHZ) and outer (OHZ) habitable zones.

Except for HD 131977 (which is an especially close-in binary and may not have dynamically stable circumstellar regions though there may be circumbinary regions of interest) all of the nearest 13 binaries feature separations greater than 24 λ/D (thus are in the super-Nyquist regime). Within 10 pc, there are 8 stars in binary systems whose separation is less than 24 λ/D – these stars on the left-hand side of the Nyquist limit line in Figure 2. Mu Cassiopeia A serves as a representative target that falls within the sub-Nyquist regime as its companion separation is approximately 19.7 λ/D.

3. MULTI-STAR WAVEFRONT CONTROL WITH WFIRST CGI

3.1 MSWC-0 and MSWC-s Modes

To enable imaging of such binary systems the diffraction and aberration-induced speckles by the off-axis companion must be suppressed simultaneously and independently of those corresponding to the on-axis star. A wavefront control system using a DM can be used to eliminate these off-axis speckles from the binary companion through the Multi-Star Wavefront Control (MSWC) technique. The principle behind MSWC is the usage of non-redundant modes on the DM being used to correct speckles. MSWC is an algorithmic method and can be used with the WFIRST CGI wavefront control with the existing DMs.

The angular separation between the stars dictates the mode of operation for MSWC. When the separation is in the sub-Nyquist regime, a dark hole can be created without any additional hardware requirements using MSWC-0. A fraction of the nearby binaries are treatable with MSWC-0 as shown in Figure 2. For the rest of the binaries at wider separations, the off-axis speckles will be outside the nominal control limit of the DM and MSWC-s must be used to remove these speckles. MSWC-s uses the control region around diffraction orders due to a grating (which can be an external grating or existing diffracting feature such as a quilting pattern on the DM surface) to suppress the off-axis speckles. The requirement for MSWC-s is therefore that an appropriate diffraction grating exists with sufficient energy and at appropriate locations to remove the off-axis speckles in the intended dark zone.

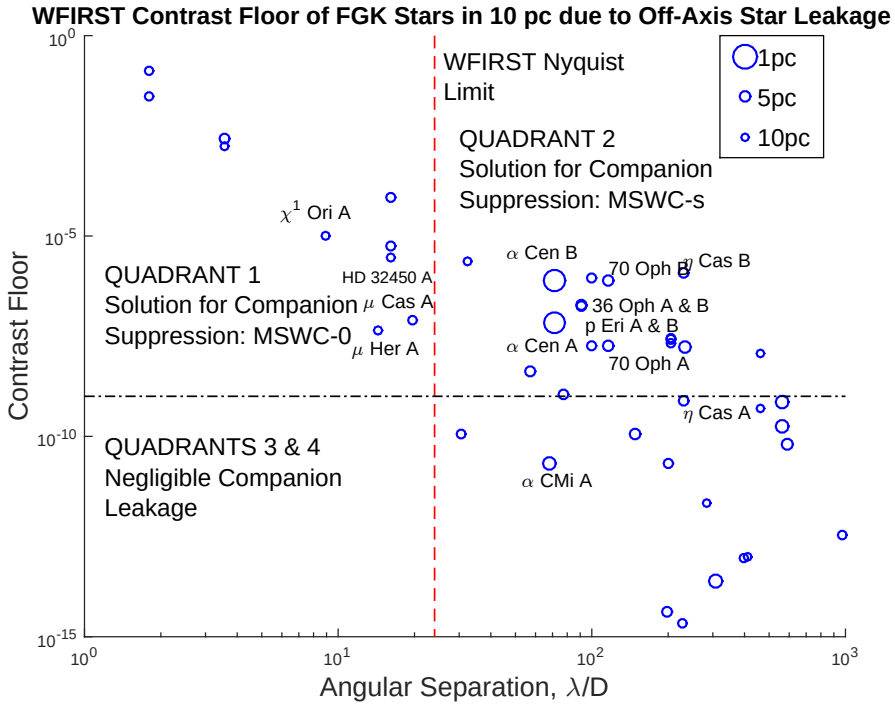

Figure 2: Computed contrast floor due to the off-axis leakage from the binary companion for WFIRST telescope assuming a nominal PSD. Also shown is the 48 x 48 DM's Nyquist-limit and the expected 1e-9 raw contrast limit.

3.2 WFIRST CGI SPC Disk Mode

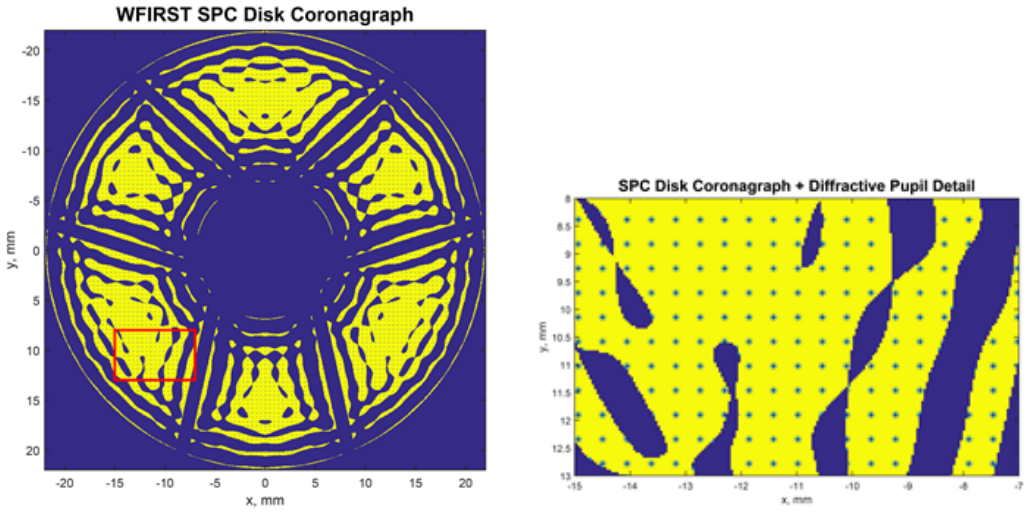

(a) (b)

Figure 3: Diffractive pupil used in this study consists of a set of non-reflecting dots superimposed on the WFIRST SPC Disk mask. There are 100 x 100 dots across the SPC covering approximately 3% area: (a) Full view of diffractive pupil with zoom-in region marked by red rectangle (b) Zoomed-in detail of diffractive pupil showing non-reflecting dots that create the diffraction orders.)

The WFIRST CGI instrument features three different coronagraphic modes using a single Lyot-style architecture:

- **Hybrid Lyot Coronagraph (HLC) Imaging Mode** featuring a 360-degree dark hole in imaging mode spanning 3-10 λ/D (fed to EMCCD camera)
- **Shaped Pupil Coronagraph (SPC) Characterization Mode** featuring a double-sided 120-degree dark hole spanning 3-8 λ/D (fed to the IFS)
- **Shaped Pupil Coronagraph (SPC) Disk Imaging Mode** featuring a 360-degree dark hole spanning 6.5-20 λ/D (fed to EMCCD camera)

MSWC can be applied with any of these imaging modes. We have identified the SPC Disk Imaging Mode as the most favourable mode to investigate MSWC operation to enable imaging Alpha Centauri system since its inner and outer working angles span the entire habitable zone of Alpha Centauri B; the outer working angle reaches out to 60% of the outermost habitable zone radius (at quadrature) for Alpha Centauri A. The WFIRST SPC Disk mask was designed for a mean contrast of 7.8×10^{-10} in 10% around 575 nm.[6] Experimental performance was recently verified in a vacuum test at HCIT to a level of 3.5×10^{-10}.[?]

The WFIRST CGI has baselined a pair of 48 x 48 Xinetics DMs for the WFC loop to enable high-contrast imaging with a double-sided ark hole and which can be operated in any of the three imaging modes. The Xinetics DMs are polished to remove quilting orders (which could have otherwise served as a diffraction grating).

3.3 Off-axis Leakage in SPC Disk Mode

Thus, to enable MSWC-s a diffractive pupil is needed to create diffractive orders. The diffractive pupil can be an identical SPC Disk Mask with a set of superimposed (non-reflecting) dots – the spacing between the dots on the diffractive pupil dictates the location of the diffraction orders in the focal plane while the size of the dots drives the strength of the diffraction orders (through the total amount of diffracted energy). The diffractive pupil used in this study is shown in Figure 3 and features 100 x 100 dots evenly spaced across the pupil thus resulting in diffraction orders spaced at 100 λ/D intervals in the focal plane. The area blocked by the dots is approximately 3% of the pupil. The overall SPC Disk mask shape can be seen in the left pane of figure 3 while in the right pane zoom-in detail the individual diffractive dots can be seen.

The corresponding off-axis PSF and leakage with the diffractive pupil can be seen in Figure 4 with the monochromatic PSF shown in the left pane and the broadband PSF in the right pane. Diffraction from the WFIRST spiders and the optimized SPC PSF controlling the WFIRST pupil diffraction can be observed around the off-axis star. Here the off-axis star is located at 110 λ/D along the horizontal and at 10 λ/D along the vertical. The nominal WFIRST SPC Disk Mask field has an inner working angle of 6.5 λ/D and an outer working angle of 20 λ/D with both indicated respectively by the white circles. For visualization purposes the field stop was set open out to a radius of 120 λ/D. Light diffracted from the field stop at the Lyot plane can still be seen at the edges of the field of view. The 100 λ/D spacing of the diffraction orders due to the diffractive pupil can be clearly observed in this figure. Additionally, leakage from the off-axis star creates a contrast floor at about the 10^{-7} contrast level across the nominal field of view. One of the first-order diffraction peaks is sufficiently close to the desired dark hole region (marked by the yellow rectangle) to be within the DM's control limit. This diffraction order peak is at the 10^{-3} contrast level. The chromatic elongation of the diffraction orders and speckles can be clearly observed in broadband light and represents the main challenge for off-axis speckle control.

The optimized on-axis SPC Disk Mask's PSF (before applying the diffractive pupil) is shown in the left pane of Figure 5. The focal-plane field stop is now set to its nominal settings shown and the simulated contrast reaches the design contrast of 7.8×10^{-10} in 10% broadband (without any on-axis aberrations). With the off-axis star at 110 λ/D as before, the (unabberrated) on-axis PSF is dominated by the off-axis companion's leakage as shown in the right pane of Figure 5.

4. SIMULATED SCENARIOS

We demonstrate the feasibility of using WFIRST SPC Disk mode for imaging multi-star systems via simulated examples. First, we demonstrate the suppression of the off-axis star only with Super-Nyquist Wavefront Control and discuss strategies for maximizing performance in broadband light. Then we consider both MSWC operating modes: MSWC-s using the Alpha Centauri system MSWC-0 using the Mu Cas geometry.

For all simulations, we use a compact model with Fresnel propagation between the DM mirrors. Initially, we considered 1-DM control. 2-DM control results are also shown demonstrating larger-size dark holes. For all simulations, a compact coronagraph architecture is considered including Fresnel propagation between the DM surfaces. In cases in which 1-DM is used the second DM is not actuated but there are chromatic effects

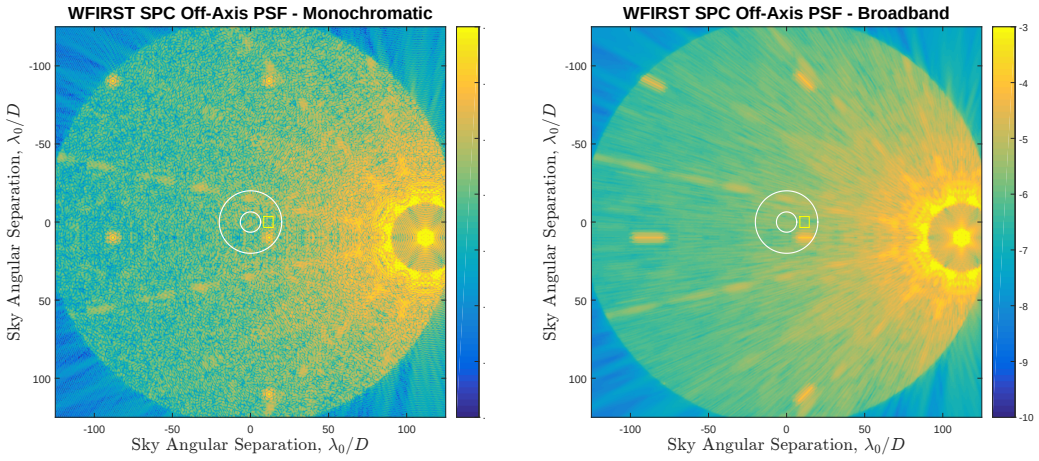

(a) (b)

Figure 4: Off-axis companion leakage with the WFIRST SPC Disk mask with the diffractive pupil. The nominal field stop (shown in white) has an outer radius of 20 λ/D. Here the field stop is set to open to show a wider field of view. Note that the leakage from the off-axis companion would not be blocked inside the region for the nominal field stop. (a) Off-axis PSF in monochromatic light (575 nm) (b) Off-axis PSF in broadband light (10%)

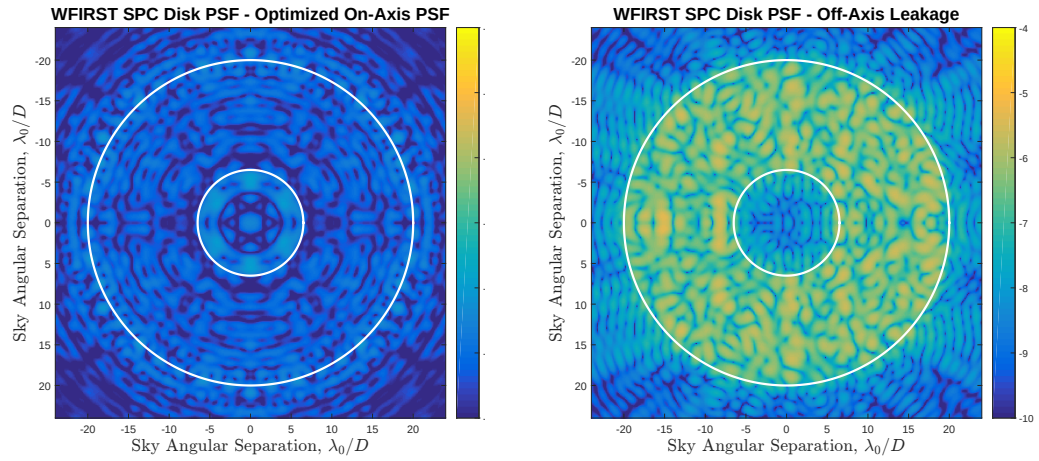

(a) (b)

Figure 5: Off-axis stellar companion leakage introduces a contrast floor before applying the diffractive pupil: (a) Optimized on-axis PSF due to SPC Disk mask (without on-axis aberrations) (b) Contrast floor due to the off-axis companion leakage.

included due to the Fresnel propagation between aberrated DM surfaces. The simulated model is idealized as no noise effects are considered (i.e., perfect estimation is assumed), no jitter is introduced during the control loop operation, and the stars are assumed to be point sources.

4.1 SNWC

The most challenging aspect of imaging wide-binaries is removal of the off-axis speckles particularly in broadband light. There are two competing effects here for an off-axis star at wide separations: (1) the further off-axis the star is the lower the contrast floor due to its leakage and diffraction contribution due to the natural PSD roll-off (2) large off-axis separations increase the broadband elongation and thus chromaticity that the DM must control for. The technique we are using to control these off-axis speckles is Super-Nyquist Wavefront Control (SNWC) detailed elsewhere.[3]

Here we consider a particular scenario where the off-axis star is located at 110 λ/D which is representative

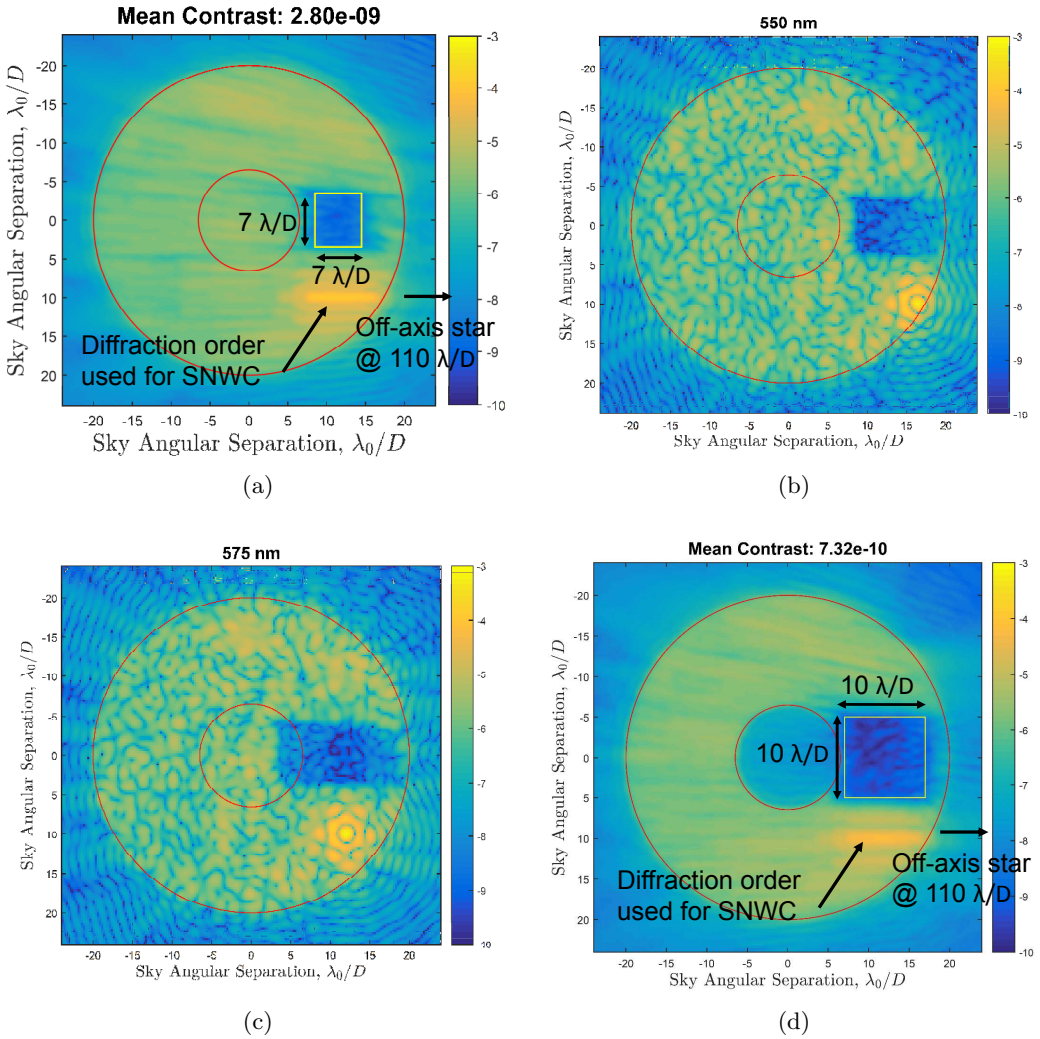

Figure 6: Super-Nyquist Wavefront Control simulation showing removal of off-axis speckles in 10% broadband (a) 1-DM control demonstrating 7×7 λ/D dark hole (b) Dark-hole corresponding to the 1-DM case at 550 nm and showing that the effective dark hole at controlled wavelengths is oversized to deal with broadband elongation (c) Dark-hole corresponding to the 1-DM case at 575 nm and showing dark hole and control order shift in the red direction (d) 2-DM control demonstrating 10×10 λ/D dark hole .

of the separation between the Alpha Centauri stars. We only consider the off-axis star to demonstrate that the off-axis speckles can indeed be controlled using the WFIRST SPC Disk mask with the diffractive pupil. Simulation results for this scenario shown in Figure 6. Only 1-DM is used to generate a dark hole spanning 7×7 λ/D in Figure 6a and achieving a mean contrast of 2.8×10^{-9}. Figure 6b and Figure 6c correspond to these same DM settings showing the dark hole in monochromatic light at 550 and 575 nm respectively. We note that the monochromatic dark hole appears extended and shifted compared to the broadband dark hole. Thus, to generate a broadband dark hole and control for the broadband-induced chromatic elongation, the dark hole must be effectively increased in size at individual wavelengths. Additionally, there is leakage and dark hole shrinkage at intermediate wavelengths at which the DM is not specifically optimizing.

To generate a larger broadband dark hole the following basic strategies can be used:

- increase degrees of freedom (e.g., use the 2-DM system)
- optimize correction wavelengths (add additional correction bands and optimally space them)
- oversize dark hole size (in combination with choosing the appropriate correction bands to ensure minimal leakage at intermediate wavelengths)
- increase energy available by using a stronger diffractive pupil (e.g., increase the size of the diffractive pupil's dots to have additional energy available in the diffractive order peak)
- optimized DM relinearization strategies (to minimize nonlinear effects associated with larger DM strokes)

Application of these strategies and especially using the 2-DM system available in the WFIRST CGI layout allows a larger dark hole as demonstrated in the simulation in Figure 6d. Here a dark hole spanning 10×10 λ/D is achieved with a deeper mean contrast of 7.3×10^{-10}. Thus when adding additional degrees of freedom and optimizing the wavefront control parameters a dark hole that is more than twice the area can be achieved in broadband.

4.2 MSWC-s

Next, we consider the additional challenge of controlling the more realistic scenario featuring both Alpha Centauri stars. Alpha Centauri A is located on-axis behind the SPC Disk mask while Alpha Centauri B is at an identical location to the SNWC scenario considered earlier. This scenario thus demonstrates MSWC-s at super-Nyquist separations. Although the WFC loop is known to be able to control the on-axis star's aberrations and it was shown that the off-axis star's speckles can also be controlled, it can be more demanding on the overall DM stroke to control both simultaneously.

As the diffractive pupil is the same and the off-axis star is also in the same location as the SNWC case, the first diffractive order used is identical both in location and peak energy to that seen in Figure 6a. A multi-star dark hole is created using 1-DM control for this configuration as shown in Figure 7. The mean contrast achieved in the 7×7 λ/D dark hole is 3.9×10^{-9} as shown in Figure 7a. The DM setting corresponding to this multi-star dark hole is shown in Figure 7b requiring 401 nm of peak-to-valley sag but only 33 nm RMS. This corresponds to an on-axis Strehl Ratio of 0.82. These DM settings were achieved within 15 iterations and required 6 relinearizations of the DM Jacobian matrix. In Figure 7c the on-axis contribution from Alpha Centauri A (with a mean contrast of 1.4×10^{-9} and in Figure 7d the off-axis contribution (with a mean contrast of $2.5 \times 10^{-}9$) from Alpha Centauri B are shown. The limiting factor on performance is the off-axis dark hole which is at a very similar level to the SNWC only control considered earlier (compare Figures 6a and 7d). However, the stroke requirements on the DM do result in additional scattered light from the PSF core into the annular region (and may require either baffling or must also be controlled by the DM).

Similarly, Figure 8 shows MSWC-s operation using 2-DM control. The mean contrast achieved in the 10×10 λ/D dark hole (which is more than twice the area of the corresponding dark hole for the 1-DM control) is 8.8×10^{-10} as shown in Figure 7a. The DM setting (for the first DM only) corresponding to this multi-star dark hole is shown in Figure 8b requiring 411 nm of peak-to-valley sag and 37 nm RMS. This corresponds to an on-axis Strehl Ratio of 0.80. The second DM is not shown but is at similar stroke levels with 453 nm peak-to-valley and

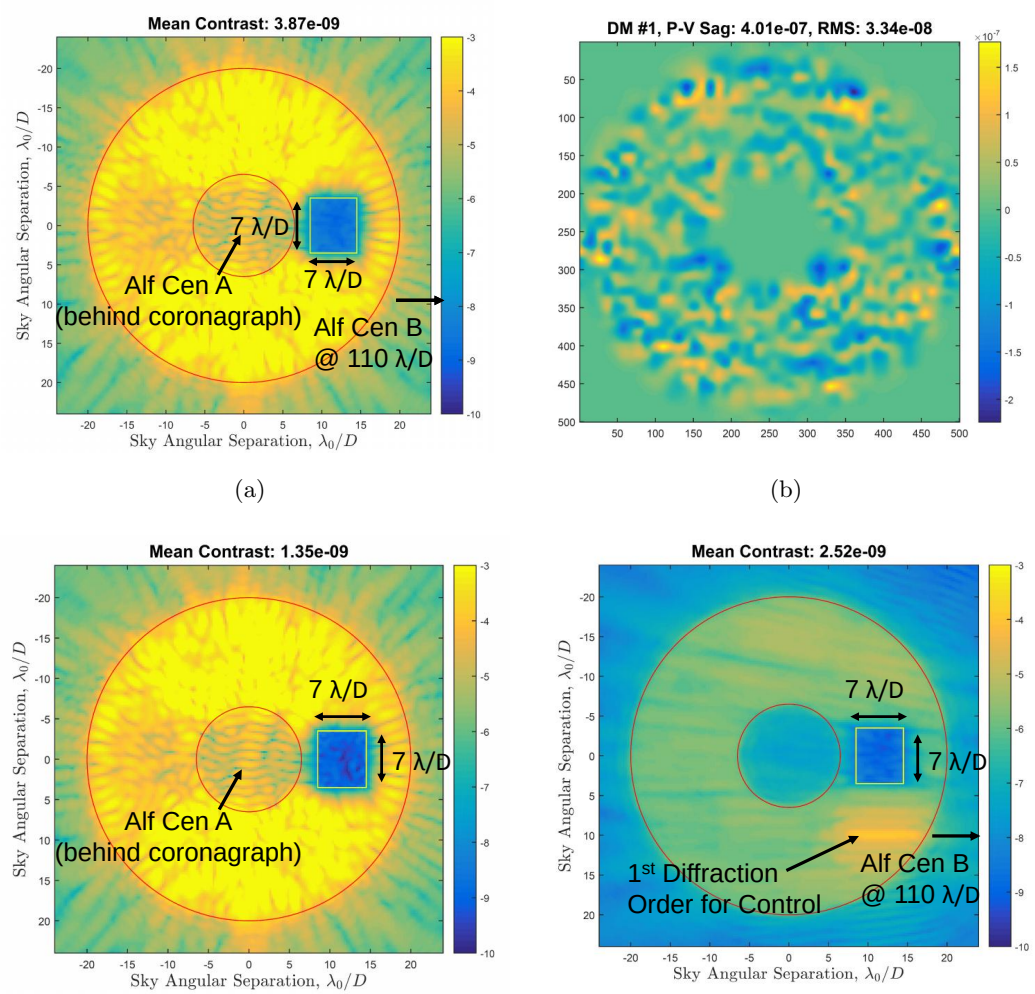

Figure 7: MSWC-s in operation for a configuration representative of Alpha Centauri using 1-DM: (a) Resulting 7×7 λ/D multi-star dark hole with a mean contrast of 3.9×10^{-9} (b) Corresponding DM sag (c) On-axis contribution (from Alpha Centauri A only) resulting in 1.4×10^{-9} mean contrast (d) Off-axis contribution resulting in 2.5×10^{-9} mean contrast.

36 nm RMS. Although the 10×10 dark hole does not encompass the full opening 6.5-20 λ/D annular opening in the nominal SPC disk field stop, this size dark hole is sufficient to image the entire 1-sided Alpha Centauri B habitable zone and out to 60% of the of Alpha Centauri's A outermost habitable zone radius (at quadrature).

4.3 MSWC-0

We also consider the case of imaging closer binaries whose separation are within the sub-Nyquist regime (i.e., MSWC-0). These binaries could be imaged without requiring a diffractive pupil in the system – this case would require only an algorithmic solution to deal with the off-axis leakage from the companion. We consider here the Mu Cassiopeia system which features binary separation of approximately $20\lambda/D$ betwen the primary and secondary components. The secondary component (an M-dwarf) is 160 times dimmer than the the primary.

The challenge with sub-Nyquist stars is that the off-axis star is now closer; its speckles are brighter and there is no coronagraph that reduces diffraction from the nearby off-axis binary. Thus the entire suppression for the off-axis star must be achieved by the DM via the WFC loop. On the other hand, the off-axis star being closer

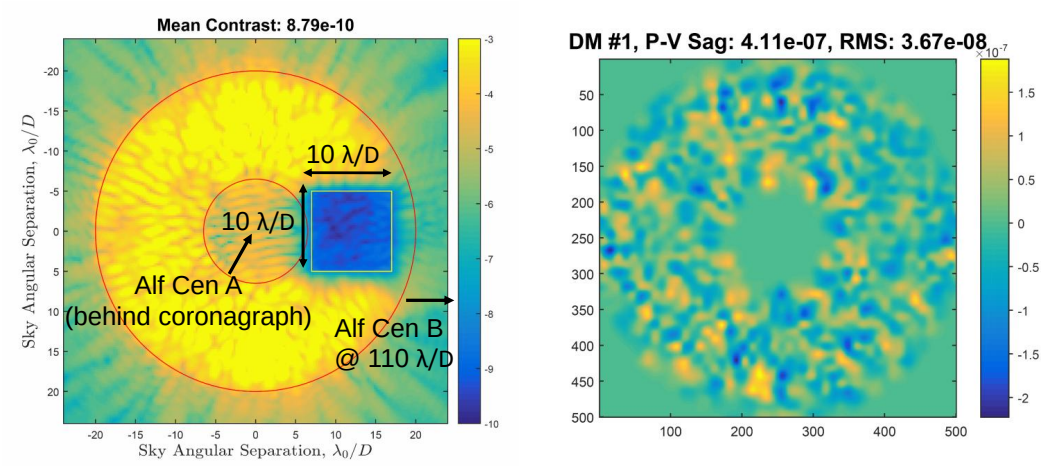

(a) (b)

Figure 8: MSWC-s in operation for a configuration representative of Alpha Centauri using 2-DMs: (a) Resulting 10×10 λ/D dark hole with a mean contrast of 8.8×10^{-10} (b) Contrast floor due to the off-axis companion leakage.

reduces the challenge of the DM needing to deal with the broadband elongation associated with speckles at wide angular separation.

Figure 8 shows MSWC-0 operation using 1-DM control. The mean contrast achieved in the 7×7 λ/D dark hole is 2.4×10^{-9} as shown in Figure 9. The DM setting corresponding to this dark hole is shown in Figure 9b with peak-to-valley sag of 622 nm and RMS sag of 38 nm. Although the peak-to-valley DM sag is higher here it is still below 1 micron, while the on-axis Strehl Ratio is 0.81 and is dominated by the RMS sag.

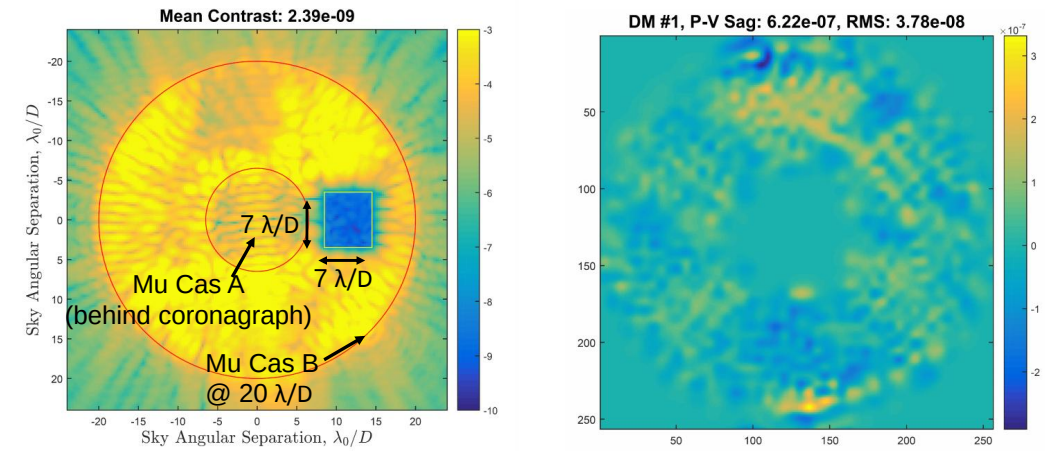

(a) (b)

Figure 9: MSWC-0 in operation for a configuration representative of Mu Cas using 1-DMs: (a) Resulting 7×7 λ/D dark hole with a mean contrast of 2.4×10^{-10} (Mu Cas B is visible at the edge of the nominal field stop's outer working angle) (b) Corresponding DM sag for the MSWC-0 dark hole.

5. CONCLUSION

In this study, we have investigated operation of the WFIRST CGI with MSWC and demonstrate that in simulation there are feasible solutions. In particular, we have explored the different coronagraphic modes available with the WFIRST CGI and identified the WFIRST SPC Disk imaging mode as the best option for imaging the habitable zone of the Alpha Centauri system. For other star systems that are more distant, MSWC could be applied with other coronagraphic modes and the outer working angle would not be as an important consideration as for Alpha Centauri.

We have shown in simulation the off-axis leakage challenge that can be expected for a binary star with the WFIRST SPC Disk mask. We are using a proposed diffractive pupil superimposed on the WFIRST SPC disk mask which provides sufficient energy at the desired location. We have also closed-loop solutions using MSWC-s for an example representative of the Alpha Centauri system. We have used the 2-DM configuration available on the WFIRST SPC to create dark holes at deep contrast levels of $8.8 \times 10^{-}10$ with $10 \times 10\lambda/D$ that can discover a large portion of the habitable zone of Alpha Centauri A and completely discover the habitable zone of Alpha Centauri B. Finally, we have also demonstrated MSWC-0 operation using Mu Cassiopeia as a representative target. This operating mode can be run as a purely algorithmic implementation requiring no diffractive pupil.

To determine optimal wavefront control settings for creating wider dark holes with MSWC as well as exploring multiple star geometries and an envelop of optical aberrations, we are planning a trade study with closed-loop wavefront control run on the Pleiades supercomputer at NASA Ames.

ACKNOWLEDGMENTS

This work was supported in part by the National Aeronautics and Space Administration's Ames Research Center, as well as the NASA Astrophysics Research and Analysis (APRA) program through solicitation NNH13ZDA001N-APRA at NASA's Science Mission Directorate. Any opinions, findings, and conclusions or recommendations expressed in this article are those of the authors and do not necessarily reflect the views of the National Aeronautics and Space Administration. This research has made use of the Washington Double Star Catalog maintained at the U.S. Naval Observatory.

REFERENCES

1. D. Des Marais, M. Harwit, K. Jucks, J. Kasting, D. Lin, J. Kunine, J. Schneider, S. Seager, W. Traub, and N. Woolf, "Remote sensing of planetary properties and biosignatures on extrasolar terrestrial planets," *Astrobiology* **2**, pp. 153–181, 2002.
2. T. D. Groff, M. J. Rizzo, Q. Gong, N. T. Zimmerman, A. M. Mandell, and M. W. McElwain, "WFIRST integral field spectrograph design and operations concept," *Proc. SPIE* **1069884**, 2018.
3. F. Malbet, J. Yu, and M. Shao, "High-dynamic-range imaging using a deformable mirror for space coronography," *Publications of the Astronomical Society of the Pacific* **107**, 1995.
4. S. Thomas, R. Belikov, and E. Bendek, "Techniques for High Contrast Imaging in Multi-Star Systems I: Super-Nyquist Wavefront Control," *ApJ* **810**(1), 2015.
5. D. Sirbu, S. Thomas, R. Belikov, and E. Bendek, "Techniques for High Contrast Imaging in Multi-Star Systems II: Multi-Star Wavefront Control," *ApJ* **849**(2), 2017.
6. D. Sirbu, R. Belikov, E. Bendek, E. Holte, A. J. E. Riggs, and S. B. Shaklan, "Prospects for exoplanet imaging in multi-star systems with starshades," *Proc. of SPIE* **104001D**, 2017.
7. A. Riggs, N. T. Zimmerman, S. B. Shaklan, J. B. Jewell, and J. Gersh-Range, "Shaped pupil coronagraph design developments for the WFIRST coronagraph instrument," *Proc. SPIE* **10400-73**, 2017.
8. D. Marx, E. CAdy, A. J. E. Riggs, C. Prada, B. Kern, B.-J. Seo, and F. Shi, "Shaped pupil coronagraph: disk science mask experimental verification and testing," *Proc. SPIE* **1069849**, 2018.